Antiferromagnetism and Metamagnetism in $ErFeCuGe_4O_{12}$

Diming Xu, Maxim Avdeev, Peter D. Battle

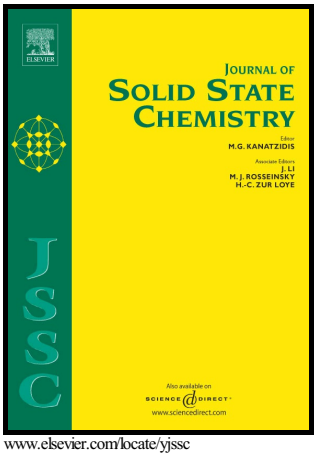

www.elsevier.com/locate/yjssc

PII: S0022-4596(18)30403-1
DOI: https://doi.org/10.1016/j.jssc.2018.09.018
Reference: YJSSC20379

To appear in: *Journal of Solid State Chemistry*

Received date: 8 August 2018
Revised date: 12 September 2018
Accepted date: 14 September 2018

Cite this article as: Diming Xu, Maxim Avdeev and Peter D. Battle, Antiferromagnetism and Metamagnetism in $ErFeCuGe_4O_{12}$, *Journal of Solid State Chemistry,* https://doi.org/10.1016/j.jssc.2018.09.018

Antiferromagnetism and Metamagnetism in $ErFeCuGe_4O_{12}$

Diming Xu[1], Maxim Avdeev[2,3] and Peter D. Battle[1,*]

1. Inorganic Chemistry Laboratory, Oxford University, South Parks Road, Oxford, OX1 3QR, U. K.
2. Australian Nuclear Science and Technology Organisation, Lucas Heights, NSW 2234, Australia
3. School of Chemistry, The University of Sydney, Sydney, NSW 2006, Australia

* to whom correspondence should be addressed: peter.battle@chem.ox.ac.uk

Abstract

Polycrystalline $ErFeCuGe_4O_{12}$ has been prepared in a solid-state reaction. It adopts a tetragonal crystal structure; space group *P*4/*nbm* with a = 9.6416(1), c = 4.7532(1) at room temperature. The Er^{3+} cations are in square-antiprismatic coordination and the Fe^{3+} and Cu^{2+} cations are disordered over one six-coordinate site. The magnetic moments of the three cations adopt an antiferromagnetic arrangement on cooling below 20 K in H = 0 kOe. The magnetic structure consists of ferromagnetic (001) sheets with the spin direction in neighbouring sheets alternating between [001] and [00$\bar{1}$] At 5 K the ordered moment of Er^{3+} was determined by neutron diffraction to be 7.90(3) μ_B and the mean moment of Fe^{3+} and Cu^{2+} was 2.43(2) μ_B. The magnetic structure is unchanged in an applied field of 10 kOe but in fields ≥20 kOe the compound begins a metamagnetic transition to a ferromagnetic structure with all atomic moments aligned along [001].

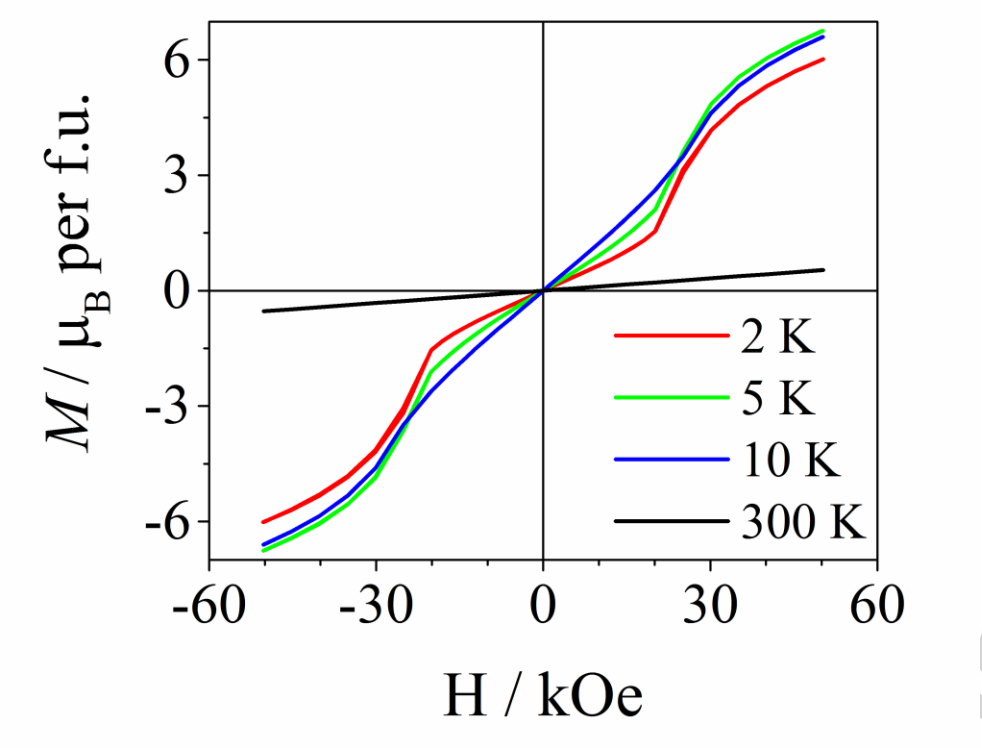

At 2 K, antiferromagnetic $ErFeCuGe_4O_{12}$ undergoes a metamagnetic transition to a ferromagnetic state in an applied magnetic field of ≥20 kOe.

Keywords: neutron diffraction; antiferromagnet; metamagnet

Introduction

Many mixed-metal germanates can be described by the general formula *ABB'*Ge_4O_{12}, where *A*, *B* and *B*' are cations of elements in the *s*, *d* or *f*-blocks of the periodic table [1-4]. Our interest centres on the subset of these compounds whose members are isostructural with tetragonal $SrNa_2P_4O_{12}$ [5]. Their crystal structure, which adopts the space group *P*4/*nbm*, consists of *xy* sheets of $[Ge_4O_{12}]^{8-}$ groups, each of which is composed of four vertex-sharing GeO_4 tetrahedra, see Figure 1. The interlayer space is occupied by the cations, which are coordinated by the oxide ions of the germanate groups. The *A* cations occupy a 2*b* site and are coordinated by eight oxide ions at the vertices of a square antiprism whereas the *B* and *B*' cations occupy a 4*f* site in a disordered manner and are octahedrally coordinated.

The magnetic properties of these germanates depend, naturally, on the identities of the cations. When *A* and *B* are both diamagnetic, as in $Y_2CoGe_4O_{12}$ ($A = B = Y^{3+}$), the compound remains paramagnetic down to a temperature of 2 K [6]. However, when *A* is diamagnetic but *B* and *B'* are magnetic, as in $CeCo_2Ge_4O_{12}$, $CeMn_2Ge_4O_{12}$ and $ZrCo_2Ge_4O_{12}$ ($B = B' = Co^{2+}$

or Mn^{2+}), antiferromagnetism or weak ferromagnetism [7, 8] is observed below a transition temperature of ≤8 K. However, these three compounds adopt three different magnetic structures, thus demonstrating the sensitivity of the magnetic behaviour to the electron configuration of the magnetic cations and the ionic radii of the diamagnetic cations. The former plays an important role in determining the direction in which the ordered spins align and the latter influences the geometry, and hence strength, of the competing superexchange interactions that are present in the structure. Long-range magnetic ordering is also observed in compositions in which the 2*b* site is occupied by a diamagnetic cation and the 4*f* site by a disordered distribution of two magnetic cations, for example Mn^{2+}/Co^{2+}, Mn^{2+}/Fe^{3+}, Co^{2+}/Ni^{2+} and Co^{2+}/Cu^{2+} [9, 10]. In an applied magnetic field of ~3-5 kOe some, but not all, of the Co^{2+}-containing compounds described above undergo a metamagnetic transition to a weakly ferromagnetic phase [7, 10]. The high-field magnetic structure of $CeCo_2Ge_4O_{12}$ is the same as the zero-field structure of $ZrCo_2Ge_4O_{12}$, demonstrating once again the sensitivity of the magnetic properties to the details of the crystal structure.

The final compounds to be considered are those in which all three cations are magnetic. We have previously reported [11] a shift from antiferromagnetism to paramagnetism, via spin-glass formation, along the series $Ln_2CoGe_4O_{12}$ where *Ln* = Tb, Dy, Ho, Er (*A* = *B* = *Ln*; *B*' = Co); those compositions that show a magnetic phase transition do so below 4 K. To date there have been no reports of isostructural compounds in which *A* is a magnetic lanthanide and *B* and *B'* are magnetic *d*-block cations. Our attempts to synthesize compounds that satisfy these criteria have not all been successful but we have now prepared $ErFeCuGe_4O_{12}$ and we describe below the results of a study of this compound by magnetometry and neutron diffraction.

Experimental

A polycrystalline sample of $ErFeCuGe_4O_{12}$ was prepared in a solid-state reaction. The appropriate stoichiometric quantities of pre-dried Er_2O_3, Fe_2O_3, CuO and GeO_2 were mixed thoroughly using an agate mortar and pestle. The mixtures were heated at 1050 °C for 4 days

with intermediate cooling and regrinding every two days. They were then pressed into pellets and annealed at the same temperature for another 10 days with cooling and regrinding every two days.

An X-ray powder diffraction (XRPD) pattern of the product was recorded at room temperature using Cu $K\alpha_1$ radiation. Neutron powder diffraction (NPD) patterns were collected using the diffractometer ECHIDNA at ANSTO. Wavelengths of 1.622 Å and 2.4395 Å were used to collect data at selected temperatures in the range $5 \leq T/K \leq 300$ with the samples contained in vanadium cans. Additional data were collected at 5 K over the magnetic field range $0 \leq H/kOe \leq 40$. When data were to be collected in an applied field the sample was pressed into relatively large pieces to prevent movement in the field, otherwise loose powders were used. The data were analysed by the Rietveld method[12] using the program GSAS[13] and the peak function developed by van Laar and Yelon [14]. Regions of the diffraction profile contaminated by scattering from the cryomagnet were excluded from the subsequent data analysis.

Magnetic measurements were performed using a Quantum Design MPMS XL SQUID magnetometer. DC susceptibility measurements were made over the temperature range $2 \leq T/K \leq 300$ in an applied field of 100 Oe after both zero-field cooling (ZFC) and field cooling (FC) of the samples. The field dependence of the magnetization was measured at selected temperatures over the field range $-50 \leq H/kOe \leq 50$ after the samples had been cooled to the measuring temperature in a magnetic field of 50 kOe. AC susceptibility data were collected over the temperature range $2 \leq T/K \leq 50$ at frequencies of 1, 10, 100 and 1000 Hz using an oscillating field of amplitude 3.5 Oe.

Results

XRPD suggested that our synthesis had produced a single-phase sample of tetragonal $ErFeCuGe_4O_{12}$. The diffraction pattern could be indexed in the space group *P*4/*nbm* (No. 125) with the unit cell parameters a = 9.6446(1), c = 4.7532(1) Å, see Figure 2. The temperature dependence of the dc molar susceptibility and the field dependence of the

magnetisation at selected temperatures are shown in Figures 3 and 4. In view of the marked temperature dependence shown by $M(H)$, the FC susceptibility was measured over the temperature range $2 \leq T/K \leq 50$ in fields in the range $0 \leq H/kOe \leq 40$, see Figure 5. When measured in an applied field of 100 Oe, $\chi(T)$ has a maximum at 20 K. The maximum broadens as the measuring field is increased and is no longer present when H >30 kOe. Fitting the Curie-Weiss law to the FC $\chi(T)$ data collected above T = 200 K resulted in values of C = 22.522(1) $cm^3\ mol^{-1}$ and θ = -8.12(2) K. The molar Curie constant of a compound containing Er^{3+}, Fe^{3+} and Cu^{2+} in a 1:1:1 ratio would be expected to be ~16.25 $cm^3\ mol^{-1}$ and the observed value thus suggests that our sample contains a magnetic impurity, albeit in too low a concentration to be detected by diffraction methods. This is consistent with the observation of weak hysteresis in the dc susceptibility at temperatures below ~110 K, see Figure 3. The temperature and frequency of the ac susceptibility is shown in Figure 6; the imaginary component is negligible throughout the measured temperature range and the real component is independent of frequency.

No impurities were apparent in the neutron diffraction pattern collected at room temperature, which, like the X-ray pattern, could be indexed in *P*4/*nbm*, see Figure 7. The structural parameters and bond lengths derived from our Rietveld analysis of these neutron data are listed in Tables 1 and 2, respectively. The same model could be used to account for a diffraction pattern collected at 30 K but additional Bragg peaks were apparent in data collected at 5 K. They could be accounted for, see Figure 8, by the antiferromagnetic structure drawn in Figure 9. The magnetic unit cell is doubled along [001] and consists of an antiferromagnetic stacking of ferromagnetic (001) layers, with the spins aligned along ±[001] which is described by the magnetic space group $P_{2c}4/nb´m´$ (#125.13.1043) [15] with **k** = (0, 0, ½). The mean ordered magnetic moments on the two cation sites are listed in Table 3. The appearance of the diffraction pattern changed again when a magnetic field greater than 10 kOe was applied. The data could be fitted, see Figure 10, by assuming the coexistence of the magnetic structures drawn in Figures 9 and 11, that is the application of an external field favoured parallel alignment of all the atomic moments, *i.e.* ferromagnetism, with a concomitant halving of the volume of the magnetic unit cell (magnetic space group P4/nb´m´, #125.7.1037, **k** = (0, 0, 0)). Figure 10 shows that with increasing field strength the intensities of the peaks characteristic of antiferromagnetic ordering, labelled **A**, decrease in intensity as those characteristic of ferromagnetic ordering, labelled **F**, increase. However, although the fraction of the ferromagnetic phase increased with field, the transition from an antiferromagnetic state to a ferromagnetic state was not complete in a field of 40 kOe. The

analysis of the in-field data was hindered by preferred orientation of the crystallites; our attempt to avoid this by using relatively large, and consequently heavy, powder particles was not as successful as it has been in the past [7]. However, reasonable agreement between the observed and calculated diffraction profiles was achieved, see Figure 10, when the preferred orientation was modelled using a March–Dollase function [16]. In order to eliminate correlations between the magnetic phase fractions and the magnitude of the ordered moment, the latter was constrained to be the same in both magnetic phases. The resulting parameters that define the magnetic behaviour are listed in Table 3. A diffraction pattern recorded when the field was returned to 0 kOe showed that the magnetic structure had returned to that drawn in Figure 9 but the preferred orientation induced by field was still present. A pattern collected after heating to 30 K contained no magnetic Bragg scattering but the same degree of preferred orientation was still observed. The bond lengths and angles derived from the data collected at 30 K on both heating and warming are listed in Table S1; the differences between them can be attributed to the shortcomings of our preferred orientation correction. The corresponding diffraction profiles are shown in Figure S1. There is a clear loss of precision in the presence of preferred orientation and it would be unwise to draw any quantitative conclusions from the data collected in a field below the transition temperature.

Discussion

Our X-ray and neutron diffraction data suggested that we had prepared a pure sample of $ErFeCuGe_4O_{12}$. However, the dc susceptibility data suggested that a low level of magnetic impurity was present. The most likely candidate is $ErFeO_3$, which is a weak ferromagnet below 640 K [17] and shows a spin-reorientation transition at 110 K [18], the latter being the temperature below which we observe a difference between the ZFC and FC susceptibilities of our sample. We estimate that a 3 wt % $ErFeO_3$ impurity in our sample would explain the relatively high value of the Curie constant determined over the temperature range $200 \leq T/K \leq 300$. The presence of this impurity does not have a significant effect on the interpretation of the remainder of our data.

The bond lengths listed in Table 1 are typical of the elements involved. At 300 K the Er – O bond length around the eight-coordinate 2*b* site, 2.314 Å, is slightly shorter than the mean length, 2.421 Å, of the eight short bonds around the A site in $ErFeO_3$ [19] and the mean 4*f* – O distance, 2.110 Å, is close to the value of 2.132 Å predicted on the basis of the bond lengths in Fe_2O_3 and CuO [20, 21]. However, the pseudo-tetragonal distortion of the octahedra, parameterized by $\langle d(4f - O2)\rangle / \langle d(4f - O1)\rangle = 0.851$, is considerably less than

that found in CuO, where all the six-coordinate sites are occupied by Jahn-Teller-active Cu^{2+} cations. The bond lengths in the GeO_4 tetrahedra are typical of those found in this structural family. The relationship between the crystal structure and the magnetic structure will be discussed in more detail below.

Both our dc and ac susceptibility data indicate that in weak fields $ErFeCuGe_4O_{12}$ is antiferromagnetic below 20 K. However, the field dependence of the susceptibility, defined as $\chi = M/H$, suggests that the antiferromagnetic ordering is lost in fields of 30 and 40 kOe, see Figure 5. Furthermore, the susceptibility is a function of field over a wide temperature range, which is also inconsistent with simple antiferromagnetic behaviour. The data shown in Figure 4 support this conclusion; at 2 K $M(H)$ shows a marked change in gradient when H~20 kOe and similar, although less pronounced, changes are observed at 5 and 10 K.

Our low-temperature neutron diffraction data allow us to offer an explanation for the magnetometry data. At 5 K, in the absence of an applied magnetic field, $ErFeCuGe_4O_{12}$ is an antiferromagnet with a unit cell that is doubled along [001]. We propose that the dominant magnetic interactions in $ErFeCuGe_4O_{12}$ are the superexchange interactions that couple the spins of NN and NNN *d*-block cations via 4*f* – O – Ge – O – 4*f* pathways, as has been discussed in detail for the case of $ZrMn_{2-x}Co_xGe_4O_{12}$ [8], and that these interactions lead to the onset of antiferromagnetic ordering at 20 K. Superexchange interactions involving the Er^{3+} cations are likely to be much weaker and it seems likely that their ordering is a consequence of the internal magnetic field within the (001) sheets of ferromagnetically aligned *d*-block cations. The ordered moments of six-coordinate Fe^{3+} and Cu^{2+} cations, as measured by neutron diffraction, are typically ~4.5 and ~0.5 μ_B, respectively [22, 23] and the mean moment of 2.43 μ_B observed at the 4*f* site is compatible with these values, thus demonstrating that both the Fe^{3+} and the Cu^{2+} cations are ordered. The value of 7.9 μ_B per Er^{3+} cation at the 2*b* site is lower than the free ion value of 9 μ_B but AlDamen *et al* [24] have shown that crystal-field effects cannot be ignored at these temperatures and the observed reduction in the moment is consistent with their calculated energy-level diagram for an Er^{3+} cation in a site of D_{4d} symmetry. The magnetic structure, in which the spins align along [001] in a doubled unit cell, differs from those adopted by the members of this structural family that have been studied previously. For example $CeMn_2Ge_4O_{12}$, $ZrMn_2Ge_4O_{12}$ and $CeMn_{1.5}Ni_{0.5}Ge_4O_{12}$, in which the spins also lie along [001], achieve antiferromagnetic order without doubling the cell volume whereas in $LnMnFeGe_4O_{12}$ (*Ln* = Y, Eu, Lu) the unit cell volume is doubled below the Néel temperature but the spins align perpendicular to [001]. The arrangement of 4*f* sites in this structure approximates to a simple cubic array with a unit cell

parameter of $a/2$. In the notation of Wollan and Koehler [25] the 4*f* sites in $ErFeCuGe_4O_{12}$ and *Ln*$FeMnGe_4O_{12}$ can thus be said to adopt an A-Type antiferromagnet arrangement, albeit with different spin directions, whereas those in $CeMn_2Ge_4O_{12}$, $ZrMn_2Ge_4O_{12}$ and $CeMn_{1.5}Ni_{0.5}Ge_4O_{12}$ adopt a C-Type arrangement. We have previously concluded [10] that subtle structural changes can cause significant changes in the relative strengths of the nearest-neighbour (NN) and next-nearest-neighbour (NNN) superexchange interactions and hence determine whether an A- or C-Type structure is adopted. We argued that A-type ordering is most likely to occur when both the ratio $<d(4f - O2)>/<d(4f - O1)>$ and the angle between the 4*f* – O1 bond and the (001) plane are low. The latter is 39.36 ° in $ErFeCuGe_4O_{12}$ and, like the bond-length ratio of 0.851, it is the lowest value seen to date in these compounds. The adoption in zero field of the magnetic structure drawn in Figure 9 is thus entirely in line with our earlier work. The reasons for the selection of a particular spin direction within either structure type are less clear. Dipolar interactions are likely to be important when the magnetic species is an isotropic d^5 cation and single-ion anisotropy has been shown to be important in compositions containing Co^{2+}. In $ErFeCuGe_4O_{12}$ the strong axial anisotropy of the Er^{3+} cations on the 2*b* sites is likely to play a dominant role.

The antiferromagnetic ground state observed in the absence of an applied field becomes unstable when a field H >20 kOe is applied and a first-order metamagnetic transition to a ferromagnetic phase occurs; in effect the spins in alternate (001) sheets rotate through 180 °. The two phases still coexist in 40 kOe, the maximum field used in our neutron-diffraction experiments. The uncertainties introduced into our data analysis by the onset of preferred orientation make a detailed comparison of the structural and magnetic parameters determined in and out of the field difficult, but it is clear that the basic crystal structure does not change. The atomic moments determined by neutron diffraction at 5 K in 0 kOe would lead to a saturation magnetisation of 10.33 μ_B per formula unit in the ferromagnetic phase. The data suggest that 70 % of the sample is ferromagnetic in a field of 40 kOe and we would therefore expect to see a magnetisation of ~7 μ_B per formula unit in this field This is in reasonable agreement with the value determined by magnetometry, see Figure 4. Metamagnetic transitions have previously been observed in antiferromagnetic $CeMn_{2-x}Co_xGe_4O_{12}$ ($1.5 \leq x \leq 2.0$) [7] and $CeCo_{1.5}Cu_{0.5}Ge_4O_{12}$ [10], but not in *Ln*$MnFeGe_4O_{12}$ up to 50 kOe [9]; they are thus only seen in compositions containing an anisotropic magnetic cation. We note that if μ = 8 μ_B, *H* = 20 kOe and T_N = 20 K, then $\mathbf{\mu.H} \sim k_B T_N$, that is the energy of interaction between the atomic moment of Er^{3+} and the applied field needed to start the transition is comparable to the thermal energy at the antiferromagnetic ordering temperature.

Conclusions

$ErFeCuGe_4O_{12}$ is isostructural with $SrNa_2P_4O_{12}$. The Er^{3+} cations occupy a site with square-antiprismatic coordination by oxygen whereas the Fe^{3+} and Cu^{2+} cations are disordered over a single, six-coordinate site. In weak magnetic fields the compound is antiferromagnetic below 20 K. All three cation species partake in the ordering, which involves an antiferromagnetic stacking of ferromagnetic sheets along [001] of the tetragonal unit cell. At 5 K, a metamagnetic transition to a ferromagnetic phase begins in an applied field H = 20 kOe and is 70 % complete when H = 40 kOe. Quantitative analysis of any structural changes induced by the field was impeded by the onset of preferred orientation in the polycrystalline sample and in order to perform a more complete study it will be necessary to grow and characterize a single-crystal of $ErFeCuGe_4O_{12}$.

Acknowledgments

We thank E. C. Hunter for assistance with the ac magnetometry measurements.

References

[1] J.A. Campa, C. Cascales, E. Gutierrez-Puebla, M.A. Monge, I. Rasines, C.R. Valero, *Journal of Solid State Chemistry* 124 (1996) 17-23.

[2] C. Cascales, M.A. Monge, *Journal of Alloys and Compounds* 344 (2002) 379-384.

[3] C. Taviot-Gueho, P. Leone, P. Palvadeau, J. Rouxel, *J. Solid State Chem.* 143 (1999) 145 - 150.

[4] H. Yamane, R. Tanimura, T. Yamada, J. Takahashi, T. Kajiwara, M. Shimada, *Journal of Solid State Chemistry* 179 (2006) 289-295.

[5] M.T. Averbuch-Pouchot, A. Durif, *Acta Crystallographica Section C-Crystal Structure Communications* 39 (1983) 811-812.

[6] X.-Q. Liu, P.D. Battle, J. Ridout, D. Xu, S. Ramos, *Journal of Solid State Chemistry* 228 (2015) 183-188.

[7] D. Xu, M. Avdeev, P.D. Battle, X.Q. Liu, *Inorg. Chem.* 56 (2017) 2750-2762.

[8] D. Xu, M. Sale, M. Avdeev, C.D. Ling, P.D. Battle, *Dalton Trans.* 46 (2017) 6921 - 6933.

[9] D. Xu, M. Avdeev, P.D. Battle, J.M. Cadogan, H. Lamont, *J. Solid State Chem.* 254 (2017) 40 - 46.

[10] D. Xu, M. Avdeev, P.D. Battle, *J. Solid State Chem.* 265 (2018) 339 - 344.

[11] D.M. Xu, M. Avdeev, P.D. Battle, D.H. Ryan, *Dalton Transactions* 46 (2017) 15778-15788.

[12] H.M. Rietveld, *Journal of Applied Crystallography* 2 (1969) 65 - 71.

[13] A.C. Larson, R.B. von-Dreele *General Structure Analysis System (GSAS)* Los Alamos National Laboratories LAUR 86-748 1994

[14] B. vanLaar, W.B. Yelon, *J. Appl. Cryst.* 17 (1984) 47-54.

[15] J.M. Perez-Mato, S.V. Gallego, E.S. Tasci, L. Elcoro, G. de la Flor, M.I. Aroyo, *Ann. Rev. Mater. Res.* 45 (2015) 217-248.

[16] W.A. Dollase, *Journal of Applied Crystallography* 19 (1986) 267-272.

[17] A. Bombik, B. Lesniewska, A.W. Pacyna, *Journal of Magnetism and Magnetic Materials* 285 (2005) 11-22.

[18] G.C. Deng, P.Y. Guo, W. Ren, S.X. Cao, H.E. Maynard-Casely, M. Avdeev, G.J. McIntyre, *Journal of Applied Physics* 117 (2015).

[19] M. Marezio, J.P. Remeika, P.D. Dernier, *Acta Crystallogr.* B26 (1970) 2008.

[20] S. Asbrink, L.J. Norrby, *Acta Crystallographica Section B-Structural Crystallography and Crystal Chemistry* B 26 (1970) 8-15.

[21] R.L. Blake, R.E. Hessevick, T. Zoltai, L.W. Finger, *American Mineralogist* 51 (1966) 123 -129.

[22] B.C. Tofield, *J. de Physique* Coll C6 (1976) 539 - 569.

[23] D. Vaknin, S.K. Sinha, D.E. Moncton, D.C. Johnston, J.M. Newsam, C.R. Safinya, H.E. King, *Physical Review Letters* 58 (1987) 2802-2805.

[24] M.A. AlDamen, S. Cardona-Serra, J.M. Clemente-Juan, E. Coronado, A. Gaita-Arino, C. Marti-Gastaldo, F. Luis, O. Montero, *Inorganic Chemistry* 48 (2009) 3467-3479.

[25] E.O. Wollan, W.C. Koehler, *Physical Review* 100 (1955) 545-563.

Figure 1 Polyhedral representation of the crystal structure of $ErFeCuGe_4O_{12}$ viewed along (a) [001] and (b) [100]: green tetrahedra and purple octahedra represent GeO_4 and $(Fe/Cu)O_6$ groups, respectively; blue circles represent Er^{3+} cations.

Figure 2 Observed (red dots) and calculated (green line) X-ray diffraction pattern of $ErFeCuGe_{412}$ at room temperature; $\lambda = 1.5406$ Å. A difference curve (purple line) is shown and reflection positions are marked by vertical bars.

Figure 3 Temperature dependence of the dc molar magnetic susceptibility of $ErFeCuGe_4O_{12}$. The data points highlighted in red in the inset were fitted to the Curie−Weiss law.

Figure 4 Field dependence of the magnetization of $ErFeCuGe_4O_{12}$ at selected temperatures

Figure 5 Field dependence of the molar magnetic susceptibility of $ErFeCuGe_4O_{12}$ at low temperatures.

Figure 6 AC molar susceptibility of $ErFeCuGe_4O_{12}$ as a function of temperature and frequency.

Figure 7 Observed (red dots) and calculated (green line) NPD pattern of $ErFeCuGe_4O_{12}$ at room temperature; $\lambda = 1.622$ Å. A difference curve (purple line) is shown and reflection positions are marked by short, vertical bars. Three low-angle peaks are labelled as **P**, **Q** and **R** for comparison with Figures 8 and 10.

Figure 8 Observed (red dots) and calculated (green line) NPD pattern of $ErFeCuGe_4O_{12}$ at 5 K; $\lambda = 2.4396$ Å. A difference curve (purple line) is shown. Magnetic (upper) and structural (lower) reflection positions are marked by short, vertical bars. Three low-angle peaks indicative of antiferromagnetic ordering are labelled **A**. An additional, unlabelled magnetic peak can be seen between **P** and **Q**.

Figure 9 Magnetic structure of $ErFeCuGe_4O_{12}$ at 5 K in the absence of an applied magnetic field.

Figure 10 Observed (red dots) and calculated (green line) NPD patterns of $ErFeCuGe_4O_{12}$ at 5 K; $\lambda = 2.4396$ Å in fields of H = (a) 10, (b) 30 and (c) 40 kOe. Difference curves (purple line) are shown. Magnetic (upper and middle) and structural (lower) reflection positions are marked by short, vertical bars. Two low-angle peaks indicative of ferromagnetic ordering are labelled **F**.

Figure 11 High-field ferromagnetic structure of $ErFeCuGe_4O_{12}$ at 5 K.

Table 1 Structural parameters of $ErFeCuGe_4O_{12}$ at room temperature and 5 K

		T	
		RT, λ = 1.622 Å	5 K, λ = 2.4395 Å
Er	U_{iso}/Å^2	0.0095(4)	0.0093(9)
Fe/Cu	U_{iso}/Å^2	0.0066(3)	0.0023(7)
Ge	*x*	0.5226(1)	0.5235(1)
	U_{iso}/Å^2	0.0046(2)	0.0028(6)
O1	*x*	-0.3674(1)	-0.3669(2)
	z	0.1869(3)	0.1858(5)
	U_{iso}/Å^2	0.0101(3)	0.0021(7)
O2	*x*	0.1575(1)	0.1575(2)
	y	0.0629(1)	0.0617(2)
	z	0.2596(2)	0.2570(4)
	U_{iso}/Å^2	0.0082(2)	0.0014(4)
a/Å		9.6416(1)	9.6408(1)
c/Å		4.7532(1)	4.7469(1)
V/Å^3		441.86(1)	441.20(1)
R_{wpr}		3.98%	6.16%
χ^2		2.385	10.41

Space group *P*4/*nbm* (No. 125), Z = 2

Er on 2*b* (¼, ¼, ½); Fe/Cu on 4*f* (0, 0, ½);

Ge on 8*k* (*x*, ¼, 0); O1 on 8*m* (*x*, -*x*, *z*); O2 on 16*n* (*x*, *y*, *z*)

Table 2 Bond lengths (Å) and bond angles (degrees) in $ErFeCuGe_4O_{12}$ at room temperature and 5 K

	T	
	RT, λ = 1.622 Å	5 K, λ = 2.4395 Å
Er-O2 × 8	2.314(1)	2.328(2)
Fe/Cu-O1 × 2	2.342(2)	2.349(3)
Fe/Cu-O2 × 4	1.994(1)	1.998(2)
O2-O2' *	3.004(2)	2.989(2)
O2-O2" *	2.624(2)	2.652(3)
Ge-O1 × 2	1.787(1)	1.779(2)
Ge-O2 × 2	1.732(1)	1.720(2)
O2- Fe/Cu-O2'	97.74(6)	96.84(10)
O2- Fe/Cu-O2"	82.26(6)	83.16(10)
O1- Fe/Cu-O2'	83.43(4)	83.46(7)
O1- Fe/Cu-O2"	96.57(4)	96.54(7)
O1-Ge-O1	108.48(11)	108.02(19)
O1-Ge-O2	105.53(5)	105.24(9)
O1-Ge-O2	108.21(7)	108.60(13)
O2-Ge-O2	120.46(9)	120.64(17)

* distances within the equatorial plane of the $(Fe/Cu)O_6$ octahedra

Table 3 Mean ordered atomic moments in $ErFeCuGe_4O_{12}$ as a function of applied magnetic field at 5 K

H/kOe	Ordered moment/ μ_B		%AF:%F
	2*b*	4*f*	
0 ↑	7.90(3)	2.43(2)	100:0
10	7.51(3)	2.44(3)	100:0
30	7.11(6)	2.15(5)	46.1(3): 53.9(3)

40	7.46(5)	1.77(5)	30.8(2): 69.2(2)
0 ↓	7.09(4)	2.28(4)	100:0

(a)

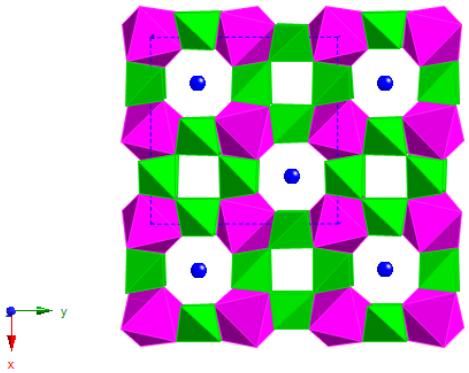

(b)

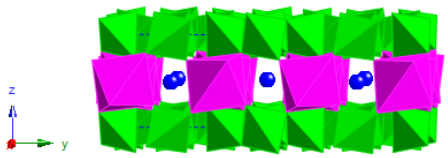

Figure 1

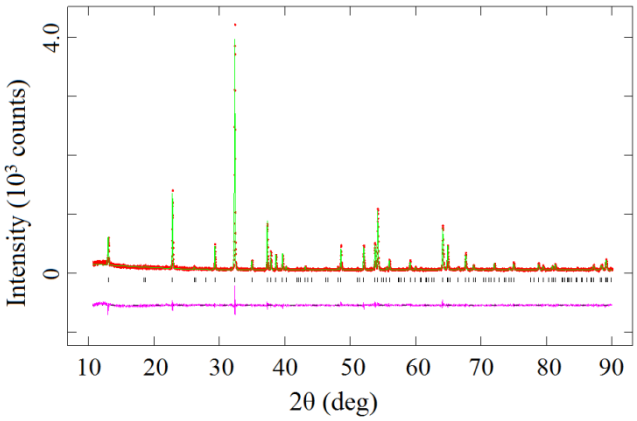

Figure 2

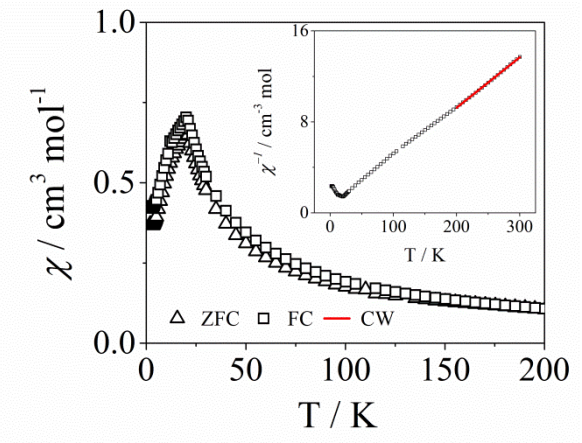

Figure 3

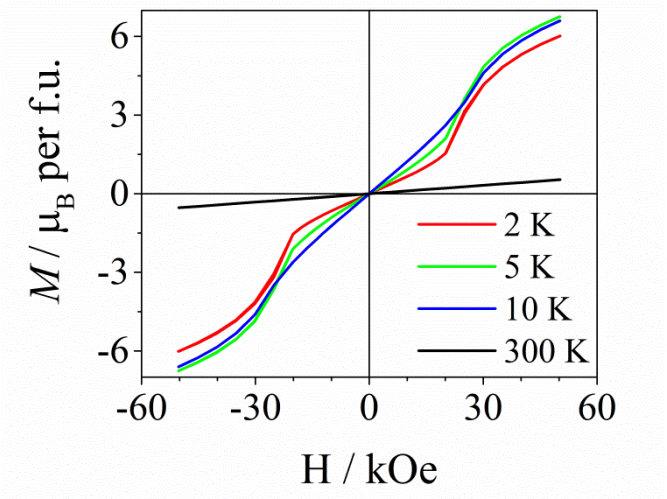

Figure 4

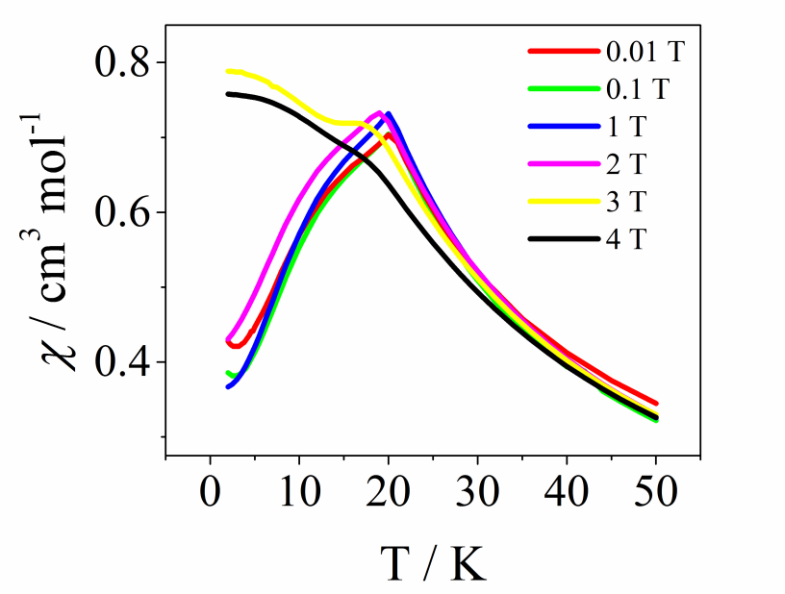

Figure 5

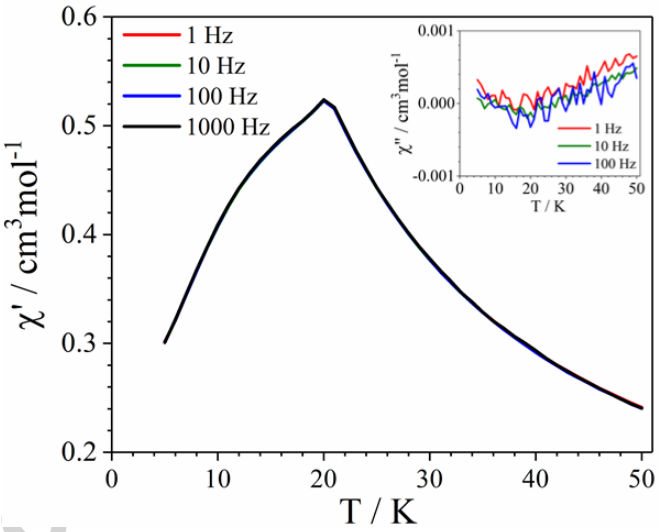

Figure 6

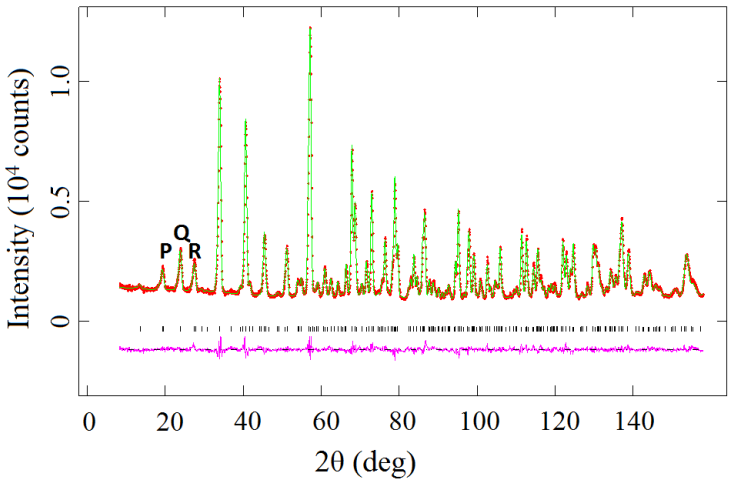

Figure 7

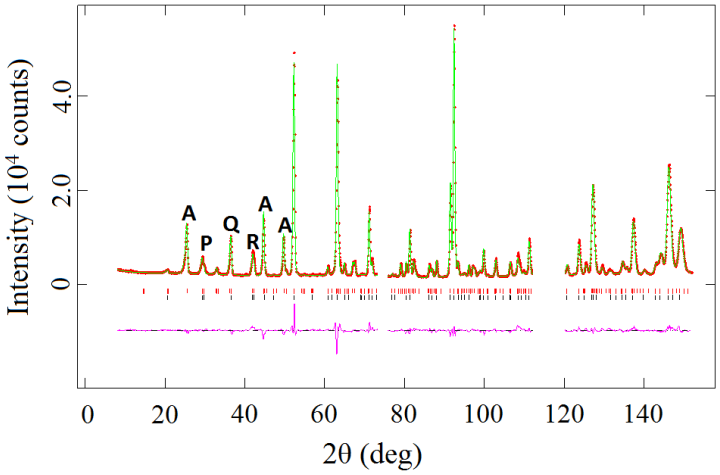

Figure 8

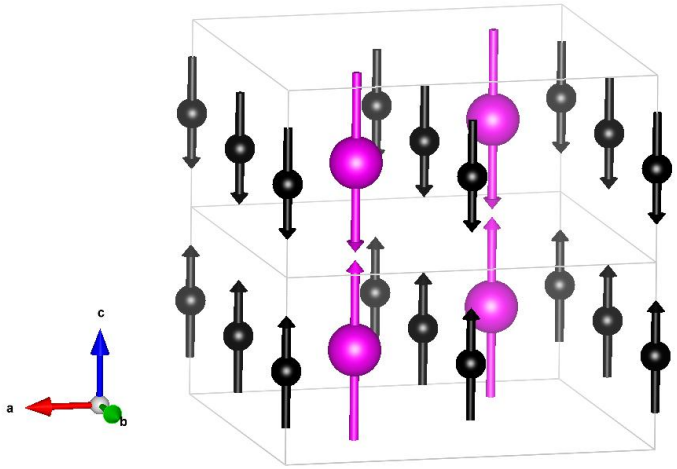
c
a
b

Figure 9

(a)

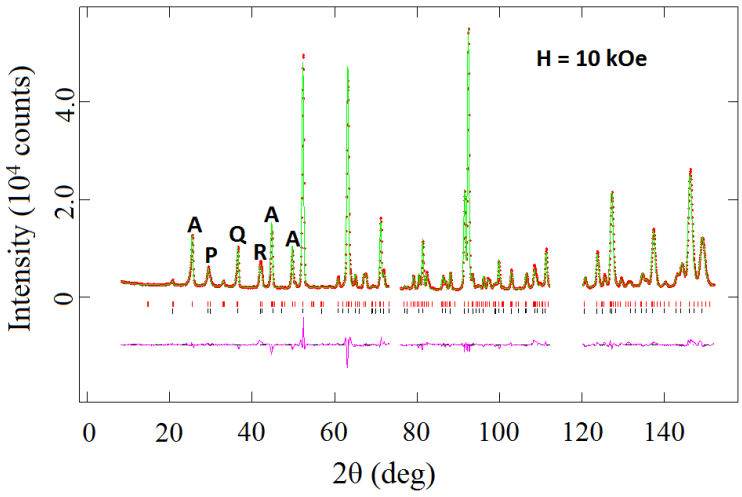
H = 10 kOe
Intensity (10^4 counts)
0
2.0
4.0
A
P
Q
R
A
A
0
20
40
60
80
100
120
140
2θ (deg)

(b)

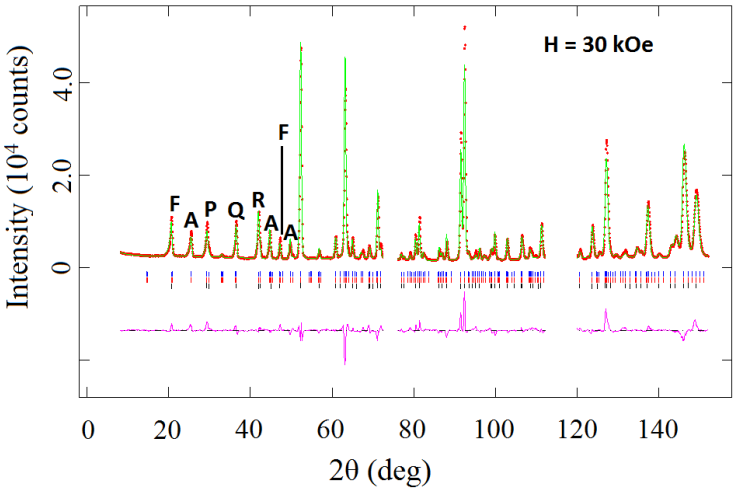
H = 30 kOe
Intensity (10^4 counts)
0
2.0
4.0
F
A
P
Q
R
A
F
A
0
20
40
60
80
100
120
140
2θ (deg)

(c)

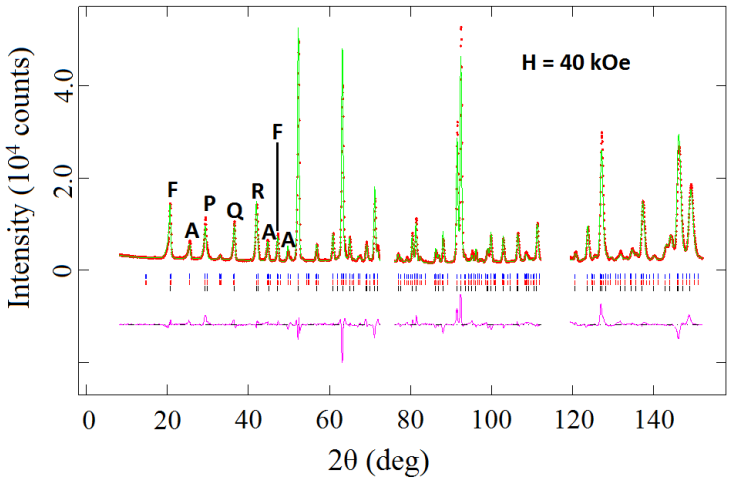
H = 40 kOe
Intensity (10^4 counts)
0
2.0
4.0
F
A
P
Q
R
A
F
A
0
20
40
60
80
100
120
140
2θ (deg)

Figure 10

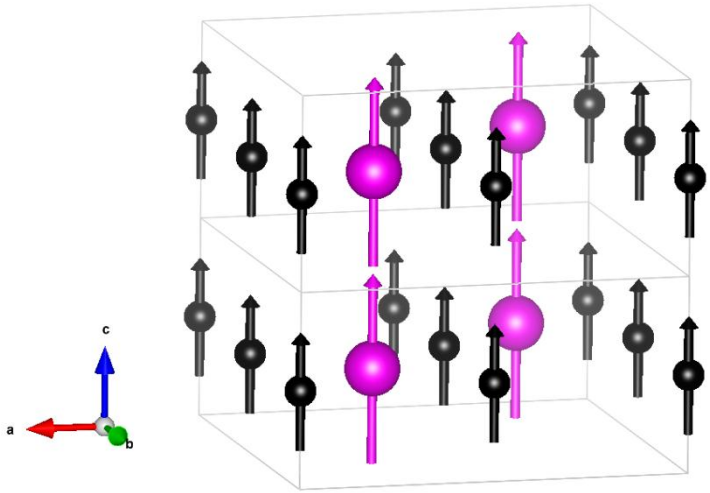
c
a
b

Figure 11

Highlights

Antiferromagnetic ordering in mixed 4*f*/3*d* system

Metamagnetic transition to ferromagnetic state

Neutron diffraction in an applied field